On the relationship between magnetic field strength and loop lengths in solar coronal active regions

R. Jain[1] and C. H. Mandrini[2]

[1] Department of Applied Mathematics, University of Sheffield, UK
e-mail: R.Jain@sheffield.ac.uk
[2] Instituto de Astronomía y Física del Espacio, CONICET-UBA, CC. 67 Suc. 28, 1428 Buenos Aires, Argentina
e-mail: mandrini@iafe.uba.ar *

Received 2005; accepted

Abstract. By assuming that coronal active regions are made up of many loops, we investigate the relationship between the average magnetic field strength and loop length for a sample of active regions observed by the Soft X-ray Telescope aboard *Yohkoh*. We use photospheric magnetic data from the Michelson Doppler Imager and compute extrapolated field lines that match the observed loops. We compare our findings with the previous study of Mandrini et al. (2000). Such studies have important implications for solar coronal heating models.

Key words. 06.13.1 Sun: magnetic fields, 06.16.2 Sun: corona

1. Introduction

Ever since it has been realised that the Sun's corona is hotter than the underlying photosphere by almost three orders of magnitude, there have been efforts to explain the origin of these conditions. Dissipation of magnetohydrodynamic (MHD) waves and dissipation of stressed, current-carrying magnetic fields are among some plausible ideas. However, the major difficulty in identifying the heating mechanism is that the small scale lengths (< 1 km) involved in coronal heating models cannot be directly verified by observations, which have spatial resolutions greater than 10^3 km.

The solar corona consists of magnetic structures with different characteristics (active regions, coronal holes etc.) and it is likely that the main physical mechanism responsible for heating the plasma in each of them is different. High resolution magnetograms together with EUV and X-ray images of the corona clearly suggest a strong connection between the magnetic field and coronal heating, but the underlying processes are yet to be identified. Many developed theories of coronal heating predict the dependence of the heating rate upon parameters such as the coronal magnetic field strength and the field line length. Therefore, in order to identify the heating mechanism, it is important to know the relationship between coronal magnetic field strength and loop length from observations.

The present study is motivated by the works by Mandrini et al. (2000), Yashiro and Shibata (2001) and Jain and Yashiro (2002). Mandrini et al. used the results of Porter and Klimchuk (1995), obtained for a sample of 47 loops observed with the Soft X-ray Telescope (SXT, Tsuneta et al. 1991) aboard *Yohkoh* to test coronal heating models. Porter and Klimchuk (1995) reported that the loop temperature is independent of the loop length, but that the pressure is inversely proportional to the loop length. Mandrini et al. carried out extrapolation studies on 14 active regions (ARs) to investigate how the mean magnetic field strength of the loops depends on their end-to-end lengths. They used photospheric magnetograms, obtained with the Michelson Doppler Imager (MDI, Scherrer et al. 1991) aboard the Solar and Heliospheric Observatory (SOHO) and also from earth for some of the ARs, to compute linear force-free and magnetostatic models and determined the averaged (over the tube volume) coronal field strength, $< B >$, in approximately a thousand of individual flux loops per AR (or tubes) with regularly spaced footpoints. They found a scaling law for the loop lengths, L (between 50-300 Mm), corresponding to the soft X-ray loops in the study by Porter and Klimchuk as: $< B > \propto L^{\delta}$ where $\delta = -0.9 \pm 0.3$. This information together with the findings of Porter and Klimchuk (1995) enabled Mandrini et al. (2000) to estimate the heating rate per unit volume as a function of $< B >$ using a quasi-static model for coronal loops, which held for their studied cases (see the discussion in Porter and Klimchuk 1991 and Démoulin et al. 2003). Then, they

Send offprint requests to: R. Jain
* C.H.M. is a member of the Carrera del Investigador Científico (CONICET)

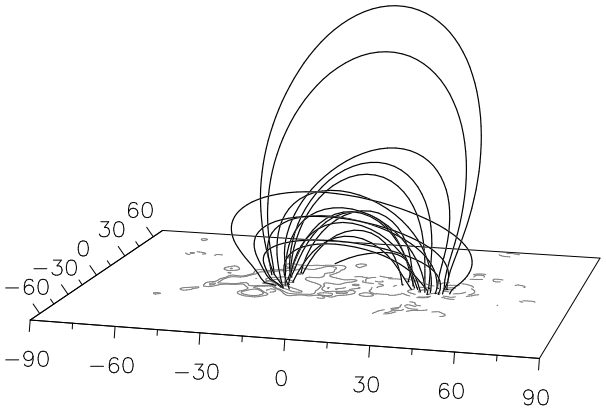

Fig. 1. Side view of the extrapolated field lines showing their height for AR7968

compared these rates derived from observations with the heating rates predicted by many theoretical coronal heating models, considering cases *with* and *without* coronal and photospheric quantities being identical. They concluded that models based on the dissipation of stressed, current-carrying magnetic fields are in better agreement with the observations than models that attribute coronal heating to the dissipation of MHD waves injected at the base of the corona. A similar conclusion was reached by the independent study of Démoulin et al. (2003). These authors used the results derived from the long-term evolution study of an isolated AR (AR 7968) by van Driel-Gesztelyi et al. (2003). The two studies, Démoulin et al. (2003) and van Driel-Gesztelyi et al. (2003), combined SXT observations of the full AR and the more precise plasma diagnostic given by the Bragg Crystal Spectrometer (BCS, Culhane et al. 1991) aboard *Yohkoh* with magnetic field measurements obtained with MDI/SOHO. They were able to analyse a larger sample of magnetic field strengths and plasma parameters in different conditions with less statistical noise.

Yashiro and Shibata (2001) (see also, Jain and Yashiro, 2002) also studied the relationship between thermal and magnetic properties of 31 mature active regions observed with SXT. In this study, the soft X-ray emission was integrated over the entire AR and a single temperature was obtained using the filter ratio. When Yashiro and Shibata (2001) (hereafter referred to as Y&S (2001)) considered the relationship between the magnetic flux density and the region size for their sample of ARs, they found that the mean magnetic flux density is independent of the region size. This led Y&S (2001) to conclude that their results were consistent with Alfvén wave heating mechanism and possibly the advanced nanoflare model proposed by Sturrock et al. (1999) for strong magnetic fields.

The opposite inference on the main coronal heating mechanism based on the results of Mandrini et al. and Y&S (2001) needs to be explained, since it is unlikely that a different main heating mechanism be at work in ARs with similar global characteristics. The explanation could

Table 1. SXT active regions and relevant parameters

Region number	NOAA number	ϕ^{a} (10^{21} Mx)	S_{AR}^{b} (Mm)	α^{c} (10^{-3} Mm^{-1})
1	8052	3.2	42	9.4
2	7968	4.0	50	-6.3
3	7961	1.3	27	0
4	7982	4.5	38	0
5	7994	0.9	33.5	0
6	8024	0.7	20	0
7	8041	0.5	31	0
8	7981	12.3	68	6.3
9	7999	15.9	77	-12.3
10	8004	9.0	62	-12.3

[a] ϕ is the unsigned magnetic flux at the photospheric level.
[b] S_{AR} is the active region size which is the flux weighted mean distance between opposite polarity photospheric fields (see the text).
[c] α is the shear parameter as shown in equation (1).

be in the different methods used for estimating the typical scale length and the magnetic flux density to derive their relationship. Unlike Mandrini et al., Y&S (2001) did not carry out extrapolation studies. The typical length scale in their work is the AR size, which is taken as the square root of its area (A). Also, the mean magnetic flux density for each coronal active region was calculated by assuming that the total photospheric magnetic flux (ϕ), measured from MDI/SOHO magnetograms at the photospheric level is same as at the coronal level. Y&S (2001) thus used the coronal active region size $A^{1/2}$ to get mean magnetic flux density as $B = \phi/A$) for each AR.

A specific aim of this paper is to carry out extrapolation studies for a set of the ARs considered by Y&S (2001), in the same way as Mandrini et al. (2000) did, and determine the relationship between loop length and average field strength on the loop if any. Such studies have important consequences for coronal heating theory. The paper is organised as follows. In Section 2, we describe the data analyses and their results. In section 3, we present our conclusions followed by a brief discussion on key issues, such as which are the more relevant scaling laws for coronal AR heating and is there a universal scaling law relating magnetic field strength and loop lengths?

2. Data Analysis and Results

All the coronal data used in this study come from full frame SXT images obtained either with the thin Al1 or A1Mg filters. For the magnetic data we use the full disc level 1.5 MDI magnetograms. These data are the average of 5 magnetograms with a cadence of 30 seconds. They are constructed once every 96 minutes. The error in the flux densities per pixel in the averaged magnetograms is ≈ 9 G, and each pixel has a mean area of 1.96 Mm^2.

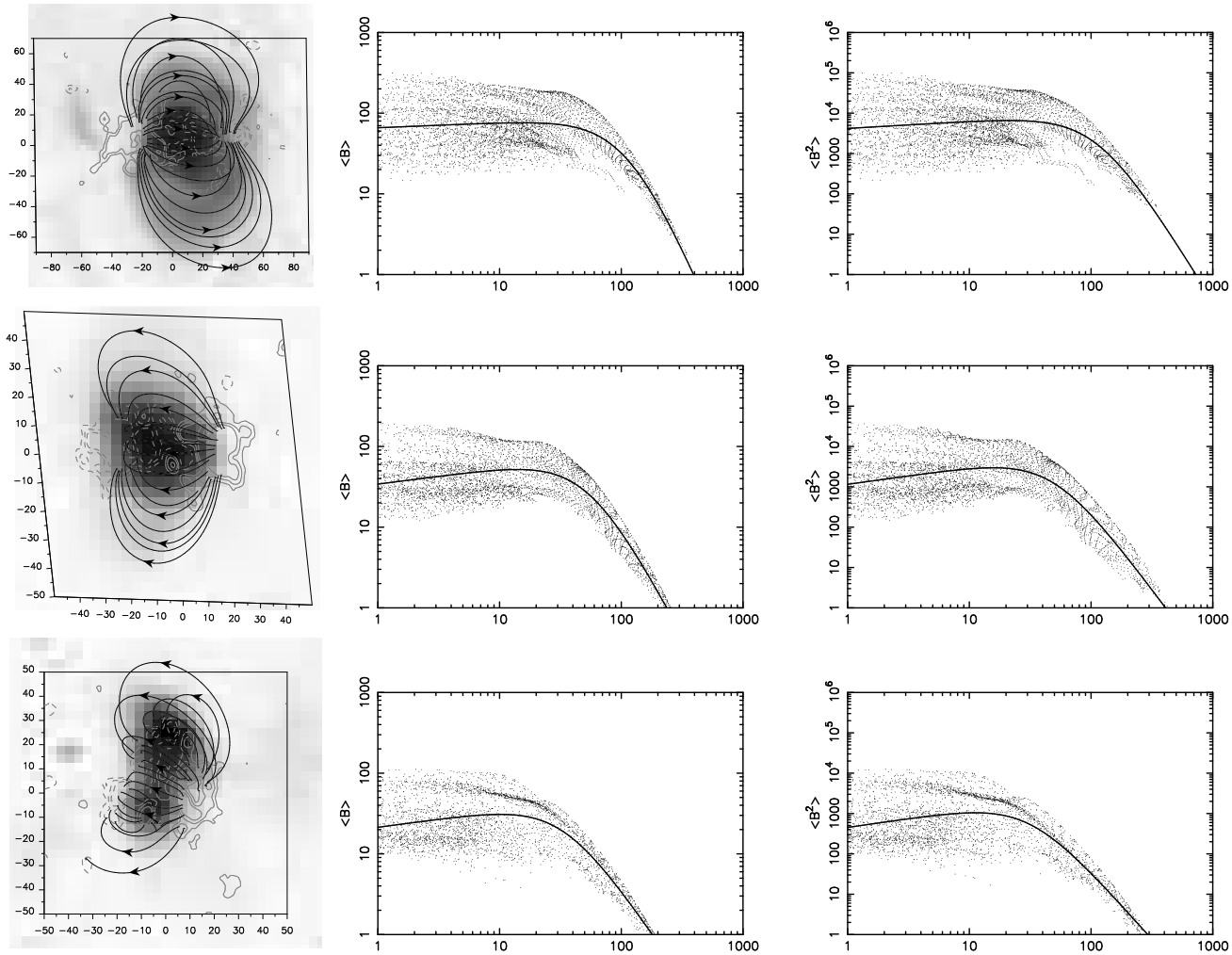

Fig. 2. First column: an overlay of an SXT image to an MDI magnetogram including computed field lines for three of the modelled ARs. From top to bottom: AR 7968 (magnetic data at 14:28 UT and SXT AlMg filter image at 18:08 UT on June 7, 1996), AR 7994 (magnetic data at 06:27 UT and SXT AlMg filter image at 06:23 UT on November 11, 1996) and AR 8024 (magnetic data at 19:13 UT and SXT AlMg filter image at 19:09 UT on March 20, 1997). Three (± 20, 50, 100 G) isocontours of the line of sight magnetic field have been drawn for AR 7994 and AR 8024 and four (± 40, 100, 500, 1000 G) for AR 7968. The x and y axes are in Mm. Second and Third column: scatter plots of $< B >$ and $< B^2 >$ for the three chosen ARs. The axes have logarithmic scales with the field line length L (abscissa) measured in Mm and the magentic field in G. Each point represents a computed field line. Figures for $< B >$ and $< B^2 >$ correspond to field lines anchored at places where the field at both footpoints is larger than 10 G. The curve in each plot is a least-square fit to the function $F_1(L)$ to the points.

The field lines are computed under the linear force-free assumption:

$$\nabla \times \mathbf{B} = \alpha \mathbf{B} \tag{1}$$

using a fast Fourier transform method (see Alissandrakis 1981 and Démoulin et al. 1997). In brief (see Mandrini et al. 2000 and Green et al. 2002 for details), the value of α is determined by an iterative process. As a first step, the field lines are computed for a given α and the mean distance between the observed SXT coronal loop (or the intensities on series of points when loops are not clearly visible) and the closest computed line is calculated. The process is repeated with iteration on α until the lowest mean distance (the best global fit) is achieved. The extrapolated field lines coincide with the soft X-ray emission observed by SXT (see Figure 2).

Figure 1 shows a side view of the computed magnetic field lines for active region AR7968; it can be clearly seen that field lines have different heights and lengths, which is what is expected for any AR.

In Table 1 we list the ARs (in order of magnetic complexity) used in this study and the important parameters obtained from observations (ϕ and S_{AR}) and magnetic field modelling (α). The quantity S_{AR} is the active region size which, in our case, is the flux weighted mean distance between opposite polarity photospheric fields given as follows (see Mandrini et al. 2000, for details):

$$S_{AR}^2 = (X_p - X_n)^2 + (Y_p - Y_n)^2;$$

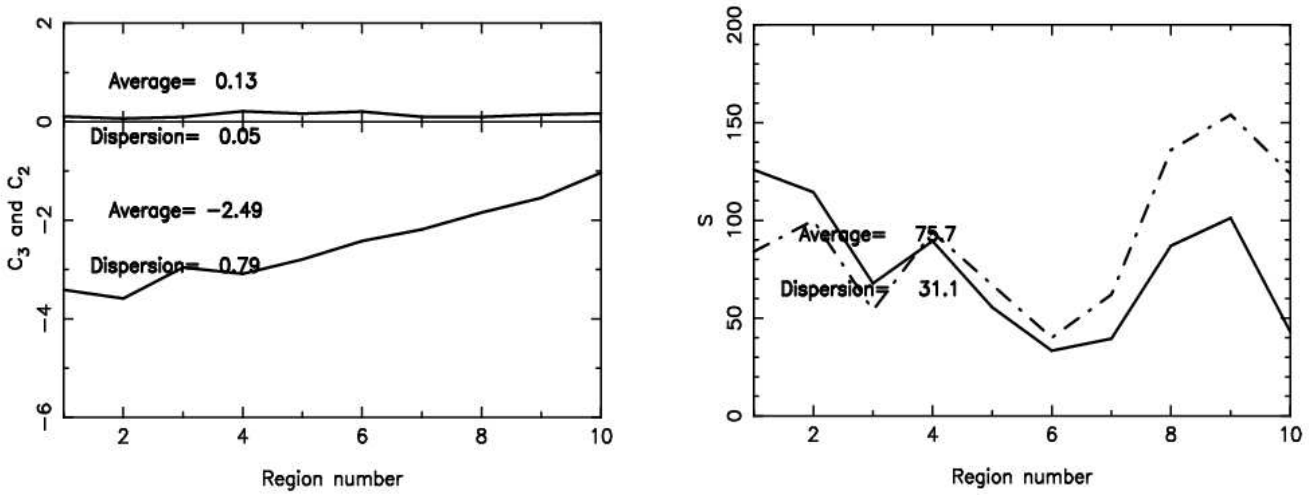

Fig. 3. Results from fitting function F_1 to $< B >$ scatter plot data from the ten ARs selected from Y&S (2001). Coefficent C_3 is plotted on the left and parameter S on the right figures, respectively. The dash-dotted line in the later figure represents the estimated active region size S_{AR} as defined in the text.

$$X_p = \frac{\sum x B_z(>0)}{\sum B_z(>0)}, \qquad Y_p = \frac{\sum y B_z(>0)}{\sum B_z(>0)}. \tag{2}$$

Similar expressions for X_n and Y_n are given for the mean position of the negative concentrations ($B_z < 0$). In both cases only vertical field strengths $|B_z| > 10$G are included to avoid noisy data.

From the modelled magnetic fields for every AR, we compute the flux-tube volume averaged magnetic quantities $< B >$ and $< B^2 >$ as (see Mandrini et al., 2000):

$$< B >= \frac{\int B dV}{\int dV} \approx \frac{L}{\int ds/B},$$
$$< B^2 >= \frac{\int B^2 dV}{\int dV} \approx \frac{\int B ds}{\int ds/B}. \tag{3}$$

where dV is the elemental volume, s is the curvilinear coordinate along the central axis of the tube, and $L = \int ds$ is the flux-tube length. Under the assumption that the variation of B within the cross section of the tube is negligible, we can replace the volume integral by a line integral using the magnetic flux conservation. Notice that $< B^2 >$ is also a measure of the magnetic energy density used in many coronal heating theories.

In Figure 2, first column, we show the extrapolated field lines superimposed on the X-ray images of three ARs. It can be seen that our models are in generally good agreement with SXT observations. The particular set of ARs chosen by Y&S (2001) are, in general, decaying ARs in which loops are cannot be individually identified. Then, our fit is not done to isolated loops but to the global SXT emission.

In order to quantify the functional dependence of $< B >$ and $< B^2 >$ on L, we follow Mandrini et al. (2000) and derive the scaling law by fitting the expression:

$$F_1(L) = C_1 + C_2 \log L + \frac{C_3}{2} \log(L^2 + S^2) \tag{4}$$

where C_1, C_2 and C_3 are constants and S is related to the AR size, as discussed in Mandrini et al. (2000), for a given active region. The least squares fit $F_1(L)$ is plotted as a solid line in Figure 2 second and third column for $< B >$ and $< B^2 >$, respectively. We have chosen the loop lengths in the interval [1,1000] Mm, and the photospheric field strength to be between [10,5000] G. Figure 2 shows that for small L, there are more data points and a larger scatter suggesting that $< B >$ and $< B^2 >$ are almost independent of L. Very low values of L are not representing real SXT coronal loops, they link mixed photospheric polarities which are at the noise level. However, we have decided to keep the full range of lenghts and magnetic field strengths to illustrate the general behaviour and also to simplify the comparison with Mandrini et al. results. On the other hand, there are fewer loops of longer lengths, and $< B >$ and $< B^2 >$ show a clear decrease with L. The qualitative behaviour seen in Figure 2 is present in all the ARs listed in Table 1. Some slight differences in the individual distributions are related to the magnetic characteristics of each AR; e.g. simple bipolar with low field, to simple bipolar with stronger field, to non-bipolar with low field, to non-bipolar with stronger field.

Figure 3 shows the parameters S, C_2, and C_3 obtained from fits to the $< B >$ versus L scatter plot data for the different ARs, these values are plotted as a function of region number from Table 1. We see from Figure 3 (left) that C_2 hovers very close to 0 in all cases, indicating that the average field strength is nearly independent of length for

Table 2. Average Values of C_3 and Correlation Factors to F_1

Averages	$< B >$	$< B^2 >$
C_3	-2.51 ± 0.80	-3.81 ± 0.96
r	0.63 ± 0.14	0.54 ± 0.16

Table 3. Average Values of the Slopes and Correlation Factors to F_2

Averages	$< B >$	$< B^2 >$
δ	-1.31 ± 0.48	-2.00 ± 0.73
r	0.71 ± 0.19	0.63 ± 0.21

$L \leq S$. C_3 ranges mostly between -3.5 and -1 and tends to be less negative for more complex regions. All these results are compatible with the results found by Mandrini et al. (2000). The parameter S (see Fig. 3, right) varies from about 40 to 130 Mm. Since in the aforementioned paper, that parameter was found to be related to some typical AR length scale we have drawn S together with S_{AR} with continuous and dash dotted line, respectively, at the right in Figure 3. It can be seen that there is a reasonably good between both parameters. We want to remark that the range of S is smaller for this set of ARs than for the set in the study by Mandrini et al. (2000), indicating that Y&S (2001) active regions are much less extended. This fact will be reflected in the range of lenghts of the loops representing the soft X-ray emission. We have done similar plots for $< B^2 >$ finding that the results are similar: a very flat distribution for $L << S$ ($C_2 \approx 0$.) and a steeply declining section for large L. The main difference is that the coefficient C_3 is more negative. The average value of C_3 for $< B >$ and $< B^2 >$ versus L scatter plot data and the quality of the least-squares fits (indicated by the Pearson's correlation factor r) are given in average in Table 2 for the ten active regions combined.

The general law discussed above involves parameters that vary from one AR to the next (primarily S and C_3). However, Mandrini et al. (2001) found a universal law based on parameters that were the same for all the cases they studied. From the scatter plots for $F_1(L)$, we have seen that this function reduces to a linear shape in the limits $L << S$ and $L >> S$. Therefore, following Mandrini et al. (2000), we will consider the simplest case of a power law, $B \propto L^{\delta}$, over limited length intervals for the loops. We fit the individual active region (taking limited intervals for the loop lengths) distributions to the function:

$$F_2(L) = C + \delta \log L \qquad (5)$$

which suggests that for $F_2 = \log B$, $B = 10^C L^{\delta}$.

The SXT loops included in the Klimchuk & Porter (1995) study had lengths in the range [50,300] Mm, which was the central range considered by Mandrini et al. (2001). However, for the particular set of ARs in this study, and because of their spatial extensions, this range is rather large. The soft X-ray emission is, in general, restricted to shorter field lines. In particular, if we compare our range for S ([40,130] Mm) to that of Mandrini et al. (2000) ([40,240] Mm) it is evident that we should modify our range of lengths to look for the value of δ. Then, we choose L in the range [50,200] Mm, which is the one representing the loops in our ARs. We take also two other modified intervals, [30,200] and [50,300]. Figures 4 (left and right) show δ as a function of AR number for these three intervals of L ([50,300], [50,200], [30,200] Mm) for $< B >$ and $< B^2 >$, respectively. For all three intervals, we take a photospheric field strength at both loop feet, B_f, above 10G.

The value found for δ for our particular set of ARs in the case of $< B >$, $\delta = -1.3 \pm 0.5$, is in very good agreement with the value taken by Mandrini et al. (2000), -0.9 ± 0.3, to represent the slope when fitting F_2 for particular ranges of lenghts in their study. This confirms that a universal law for the scaling of $< B >$ with L exists.

3. Discussion and Conclusions

Our analysis inicates that there exists a universal power law of $< B >$ and $< B^2 >$ and L for solar coronal active region loops. The power law of the form L^{δ} provides a good statistical fit for both $< B >$ and $< B^2 >$ in a limited range of lengths. This range of L obviously depends on the size of the active regions we are considering. Notice that because of our shorter range of active regions sizes, we have to shift down the range of lenghts that we take to derived the power law index δ. However, even with a different range of lenghts, but still taking that range around the active region size, the value of δ does not show any significant change due to complexity of the active regions in our set.

In order to find a value for δ that could represent the 24 ARs, 10 from our study and 14 from the study by Mandrini et al. (2000), we recomputed δ for the same three ranges of lenghts as those taken by Mandrini et al. (2000), noticing that the dispersion of δ increase for our 10 ARs in this case. We combine the 24 ARs in a single set, and we found that $\delta = -1.07 \pm 0.43$ for $< B >$ and -1.64 ± 0.70 for $< B^2 >$. If we use any of these δ values to derive the scaling law of the heating rate with L for different coronal heating models, we will find the same law within error bars when using a quasi-static model for the coronal loops. This then clearly suggests that the heating mechanism is not different for different ARs although when the ARs are smaller, weaker and decaying, the physical properties are slightly difficult to evaluate and the data have larger errors (notice that our δ value has a larger dispersion than that determined by Mandrini et al (2000)).

Finally, findings of studies like the one described here when combined with quasi-static models of coronal loops, to derived heating-rate scalings for coronal heating models, should be used with care. Observations from the Extreme Ultraviolet Imaging Telescope (EIT/SOHO) and the Transition Region and Coronal Explorer (TRACE)

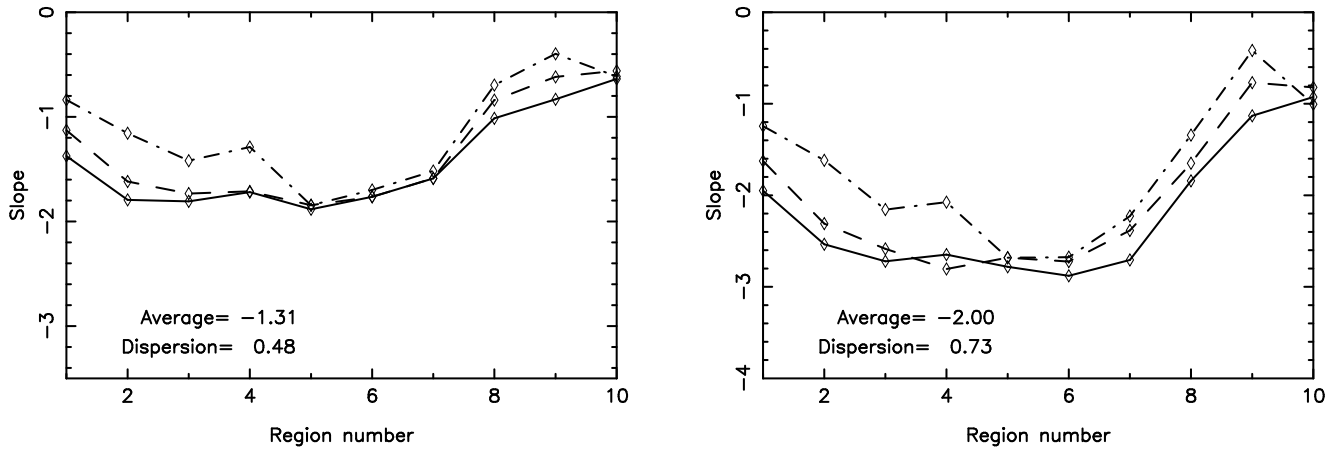

Fig. 4. Results from fitting the linear function F_2 to the scatter plot data from the ten ARs in Table 1. The slope δ is plotted against the active region number for $< B >$ and $< B^2 >$. The solid curve is for the range of lenghts [50,200] Mm, while the dash-dotted and dashed curves are for the ranges [30,200] and [50,300], respectively.

suggest that many loops with temperatures around 1 MK are not in static equilibrium. Some are seen to evolve rapidly and even those that appear steady tend to have densities much higher than can be explained by equilibrium theory (Aschwanden et al. 2000). Aschwanden et al. (2001) found that about one-third of the TRACE loops in their study can be explained by equilibrium models if the heating is sufficiently concentrated near the foot points, but two-thirds cannot be. Winebarger et al. (2003) suggest that the fraction compatible with equilibrium may actually be smaller. SXT observe loops that are generally much hotter than 1 MK. In addition to being hotter, they are also broader and fuzzier in appearance, which is not an artifact of the instrumental resolution. Furthermore, TRACE and EIT loops are overdense relative to equilibrium, SXT loops either have the correct density or are underdense. As described in Porter and Klimchuk (1995), most SXT loops are compatible with equilibrium for reasonable values of the filling factor. This indicates that, while there can be no guarantee that SXT loops are in quasi-static equilibrium, the observations are consistent with such an interpretation. For these kind of loops our results will lead to the same conclusions as those of Mandrini et al. (2000) and Démoulin et al. (2003) concerning the coronal heating models that are in better agreement with observed data.

Acknowledgements. We thank Dr. S. Yashiro for providing us his active region list and SXT observations. RJ acknowledges *The Nuffield Foundation* for NUF-NAL 04 award. We are also grateful to *The Royal Society* for their financial support. We thank the SOHO/MDI consortium for the magnetic field data and the YOHKOH Team for SXT data. SOHO is a joint project by ESA and NASA. C.H.M. thanks the Argentinean grants: UBACyT X329 and PICT 12187 (ANPCyT).

References

Alissandrakis, C. E. 1981, A&A, 100, 197
Aschwanden, M. J. 2000, ApJ, 531, 1129
Aschwanden, M. J., Schriver, C. J. & Alexander, D. 2001, ApJ, 550, 1036
Culhane, J. L., Bentley, R. D., Hiei, E., Watanabe, T., Doschek, G. A., et al. 1991, Solar Phys. 136, 89.
Démoulin, P., Bagalá, L. G., Mandrini, C. H., Hénoux, J. C., and Rovira, M. G. 1997, A&A, 325, 305
Démoulin, P., van Driel-Gesztelyi, L., Mandrini, C. H., Klimchuk, J. A., Harra, L. 2003, ApJ, 586, 592.
Green, L. M., 2002, Solar Phys., 208, 43
Jain, R., & Yashiro, S. 2002, A&A, 394, 1111
Mandrini, C. H., Démoulin P. & Klimchuk, J. A. 2000, ApJ, 530, 999
Porter, L. J. & Klimchuk, J. A. 1995, ApJ, 454, 499
Scherrer P.H., Bogart R.S., Bush R.I., Hoeksema J.T., Kosovichev A.G., et al. 1995, Solar Phys., 162, 129
Sturrock, P.A. 1999, ApJ, 521, 451
Tsuneta S., Acton, L., Bruner, M., Lemen, L., Brown, W., et al. 1991, Solar Phys., 136, 37
van Driel-Gesztelyi, L., Démoulin, P., Mandrini, C. H., Harra, L., Klimchuk, J. A. 2003, ApJ, 586, 579.
Winebarger, A. R., Warren, H. P. & Mariska, J. T. 2003, ApJ, 587, 439
Yashiro, S. & Shibata, K. 2001, A&A, 550, L113-L116